

Intrinsic ferromagnetic axion states and a single pair of Weyl fermions in the stable-state $\text{MnX}_2\text{B}_2\text{T}_6$ -family materials

Yan Gao^{1,*}, Weikang Wu^{2,3}, Ben-Chao Gong⁴, Huan-Cheng Yang⁴, Xiang-Feng Zhou¹, Yong Liu¹, Shengyuan A. Yang³, Kai Liu⁴, and Zhong-Yi Lu^{4†}

¹State Key Laboratory of Metastable Materials Science and Technology and Key Laboratory for Microstructural Material Physics of Hebei Province, School of Science, Yanshan University, Qinhuangdao 066004, China

²Key Laboratory for Liquid-Solid Structural Evolution and Processing of Materials (Ministry of Education), Shandong University, Jinan, Shandong 250061, China

³Research Laboratory for Quantum Materials, Singapore University of Technology and Design, Singapore 487372, Singapore and

⁴Department of Physics and Beijing Key Laboratory of Opto-electronic Functional Materials & Micro-nano Devices, Renmin University of China, Beijing 100872, China

(Dated: October 19, 2022)

The intrinsic ferromagnetic (FM) axion insulators and Weyl semimetals (WSMs) with only single pair of Weyl points have drawn intensive attention but so far remain rare and elusive in real materials. Here, we propose a new class of $\text{MnX}_2\text{B}_2\text{T}_6$ -B ($X=\text{Ge, Sn, or Pb}$; $B=\text{Sb or Bi}$; $T=\text{Se or Te}$) family that is the stable structural form of this system. We find that the $\text{MnX}_2\text{B}_2\text{T}_6$ -B family has not only the intrinsic FM axion insulators $\text{MnGe}_2\text{Bi}_2\text{Te}_6$ -B, $\text{MnSn}_2\text{Bi}_2\text{Te}_6$ -B, and $\text{MnPb}_2\text{Bi}_2\text{Te}_6$ -B, but also the intrinsic WSM $\text{MnSn}_2\text{Sb}_2\text{Te}_6$ -B with only a single pair of Weyl points. Thus, the $\text{MnX}_2\text{B}_2\text{T}_6$ -B family can provide an ideal platform to explore the exotic topological magnetoelectric effect and the intrinsic properties related to Weyl points.

Introduction: The discovery of the intrinsic antiferromagnetic (AFM) topological insulator (TI) MnBi_2Te_4 has attracted intensive attention in recent years [1–13]. On one hand, it has tunability in layer thickness and external magnetic field as well as various novel magnetic topological phases such as the quantum anomalous Hall insulators [2, 4], the axion insulators (AXIs) [5–7], and the magnetic Weyl semimetals (WSMs) [4, 5]. On the other hand, its unique way of introducing magnetism can provide new insights and vitality in the search for materials with coexisting long-range magnetic order and nontrivial band topology. The MnBi_2Te_4 is formed by inserting an electrically neutral [MnTe] atomic layer into its parent TI Bi_2Te_3 , which avoids the introduction of additional charges of magnetic impurity atoms and only introduces the magnetism of Mn^{2+} ions. But, the intrinsic A-type AFM MnBi_2Te_4 can only realize the AFM axion insulator state and the Weyl semimetal state with only a pair of Weyl points (WPs) under external magnetic field [5, 14]. It is worth noting that the ferromagnetic (FM) axion insulators have recently been proposed as an ideal platform to achieve desirable topological magnetoelectric responses [15], while the ideal Weyl semimetals [16] with the minimum number of WPs can serve as the simplest template to study the intrinsic physical properties of the WPs and the application of related devices based on the WPs. However, the practical materials with the intrinsic FM axion insulators [17, 18] and intrinsic WSM states with only a pair of Weyl fermions [19] have so far been very rare.

Inspired by MnBi_2Te_4 , in our previous work we de-

signed a class of magnetic axion insulators $\text{MnX}_2\text{B}_2\text{T}_6$ -A ($X=\text{Ge, Sn, or Pb}$; $B=\text{Sb or Bi}$; $T=\text{Se or Te}$) family [18], which is composed of the parent TI $X_2\text{B}_2\text{T}_5$ -A family and [MnTe] atomic intercalation. However, we found that the parent material $X_2\text{B}_2\text{T}_5$ family possesses two distinct stacking phases. Taking $\text{Pb}_2\text{Bi}_2\text{Te}_5$ as an example, both experiments [20, 21] and theory [22, 23] confirm that it has two different stacking sequences A (-Te-Pb-Te-Bi-Te-Bi-Te-Pb-Te-) and B (-Te-Bi-Te-Pb-Te-Pb-Te-Bi-Te-), labeled as $\text{Pb}_2\text{Bi}_2\text{Te}_5$ -A and $\text{Pb}_2\text{Bi}_2\text{Te}_5$ -B, respectively, and the $X_2\text{B}_2\text{T}_5$ and $\text{MnX}_2\text{B}_2\text{T}_6$ families also adopt similar labels to distinguish these two different stacking sequences. We can see that the difference between $X_2\text{B}_2\text{T}_5$ -A and $X_2\text{B}_2\text{T}_5$ -B is that the X (Ge, Sn, or Pb) and B (Sb or Bi) atoms have exchanged positions with each other [see Figs. 1(a) and 1(b)], so the [XT] atomic layer of $X_2\text{B}_2\text{T}_5$ -A is in the outermost layer, while the [XT] atomic layer of $X_2\text{B}_2\text{T}_5$ -B in the innermost layer. Previous studies [22] have shown that $\text{Pb}_2\text{Bi}_2\text{Te}_5$ -B is the stable structural form of $\text{Pb}_2\text{Bi}_2\text{Te}_5$ -A in the range of temperatures 1000 K, and the two stacking phases show significant differences in electronic properties. Then one may naturally ask whether the $\text{MnX}_2\text{B}_2\text{T}_6$ -B family obtained by inserting the [MnTe] atomic layer into the stable parent TI $X_2\text{B}_2\text{T}_5$ -B material is the stable structure with lower energy than the $\text{MnX}_2\text{B}_2\text{T}_6$ -A family? Could there be a new topological phase in $\text{MnX}_2\text{B}_2\text{T}_6$ -B due to the structural difference between the $\text{MnX}_2\text{B}_2\text{T}_6$ -B and $\text{MnX}_2\text{B}_2\text{T}_6$ -A families?

In this work, we systematically investigate the stability, magnetic, electronic and topological properties of the $\text{MnX}_2\text{B}_2\text{T}_6$ -B family by first-principles electronic structure calculations. Our calculations indicate that the $\text{MnX}_2\text{B}_2\text{T}_6$ -B family has indeed a stable structure with lower energy than the $\text{MnX}_2\text{B}_2\text{T}_6$ -A fam-

* yangao9419@ysu.edu.cn

† zlu@ruc.edu.cn

ily. Surprisingly, we find not only a series of intrinsic ferromagnetic (FM) axion insulators $\text{MnGe}_2\text{Bi}_2\text{Te}_6\text{-B}$, $\text{MnSn}_2\text{Bi}_2\text{Te}_6\text{-B}$, and $\text{MnPb}_2\text{Bi}_2\text{Te}_6\text{-B}$, but also an intrinsic Weyl semimetal (WSM) $\text{MnSn}_2\text{Sb}_2\text{Te}_6\text{-B}$ with only a pair of Weyl fermions, which has not been reported in the $\text{MnX}_2\text{B}_2\text{T}_6\text{-A}$ family. We further investigate the effect of lattice strain on the topological properties of the $\text{MnSn}_2\text{Sb}_2\text{Te}_6\text{-B}$ bulk materials. Compared with the MnBi_2Te_4 and the $\text{MnX}_2\text{B}_2\text{T}_6\text{-A}$ family, the $\text{MnX}_2\text{B}_2\text{T}_6\text{-B}$ family can provide a more ideal platform for future experiments to explore the unique topological quantum physics of the FM axion insulators and WSMs.

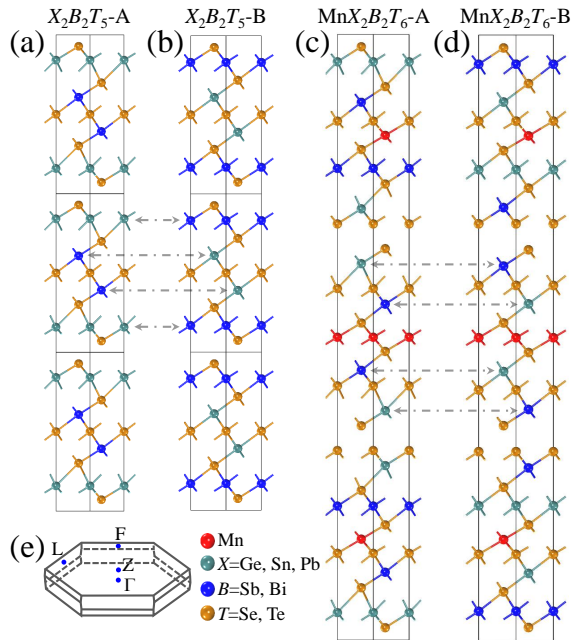


Figure 1. (Color online) Optimized crystal structures of the $\text{MnX}_2\text{B}_2\text{T}_6$ ($X=\text{Ge}$, Sn , or Pb ; $B=\text{Sb}$ or Bi ; $T=\text{Se}$ or Te) and its parent $X_2B_2T_5$ materials. The $1 \times 1 \times 3$ supercells of (a) $X_2B_2T_5\text{-A}$ and (b) $X_2B_2T_5\text{-B}$ in stacking sequences A and B, respectively. Conventional cells of (c) $\text{MnX}_2B_2T_6\text{-A}$ and (d) $\text{MnX}_2B_2T_6\text{-B}$ in stacking sequences A and B, respectively. (e) Brillouin zone (BZ) of the primitive cell of $\text{MnX}_2B_2T_6\text{-B}$.

The electronic structures of the $\text{MnX}_2\text{B}_2\text{T}_6\text{-B}$ ($X=\text{Ge}$, Sn , or Pb ; $B=\text{Sb}$ or Bi ; $T=\text{Se}$ or Te) family were investigated with the projector augmented wave method [24] as implemented in the VASP package [25] in the framework of density functional theory (DFT). The generalized gradient approximation (GGA) of the Perdew-Burke-Ernzerhof (PBE) type [26] was adopted for the exchange-correlation functional. The zero damping DFT-D3 method [27] was chosen for the interlayer vdW interaction. The PBE+ U method was utilized to treat the localized $3d$ orbitals of Mn by selecting $U=4.0$ eV. The $6 \times 6 \times 6$, $8 \times 8 \times 8$ and $12 \times 12 \times 1$ k-point meshes [28] were adopted for the primitive cell calculations of the AFM bulks, FM bulks, and the monolayers, respectively. An 18 Å vacuum layer was used to

avoid the residual interactions between neighboring image layers. The energy and force convergence criteria were set to 10^{-6} eV and 0.001 eV/Å, respectively. The phonon spectrum calculations were performed by using the DS-PAW software integrated in the Device Studio program [29], in which the $4 \times 4 \times 1$ supercell was used for the monolayer structures. The topological properties of the $\text{MnX}_2\text{B}_2\text{T}_6\text{-B}$ family were calculated by using the Wannier90 [30] and WannierTools [31] packages. An *ab initio* evolutionary algorithm, as implemented in the US-PEX code [32, 33], was employed to search for the stable bulk compounds of the $\text{MnPb}_2\text{Bi}_2\text{Te}_6$ system.

Results: To investigate the structural stability of the $\text{MnX}_2\text{B}_2\text{T}_6\text{-B}$ family, we have calculated the phonon spectra of the $\text{MnX}_2\text{B}_2\text{T}_6\text{-B}$ monolayers and bulks. As shown in Figs. S1 and S2 of Supplemental Material (SM), there are no soft phonon modes in the whole Brillouin zone (BZ), indicating that $\text{MnGe}_2\text{Sb}_2\text{Te}_6\text{-B}$, $\text{MnGe}_2\text{Bi}_2\text{Te}_6\text{-B}$, $\text{MnSn}_2\text{Sb}_2\text{Te}_6\text{-B}$, $\text{MnSn}_2\text{Bi}_2\text{Te}_6\text{-B}$, and $\text{MnPb}_2\text{Bi}_2\text{Te}_6\text{-B}$ are dynamically stable. Next, we mainly focus on these seven $\text{MnX}_2\text{B}_2\text{T}_6\text{-B}$ bulk compounds.

Considering that the interlayer Mn-Mn distance in the $\text{MnX}_2\text{B}_2\text{T}_6\text{-B}$ bulk is very large (~ 20 Å) and interrupted by the vdW gap, we first consider the various magnetic structures in their monolayers (see Fig. 1 in Ref. [18]) and then check the interlayer magnetic coupling to determine the magnetic ground states of the $\text{MnX}_2\text{B}_2\text{T}_6\text{-B}$ compounds. In our previous work on $\text{MnX}_2\text{B}_2\text{T}_6\text{-A}$, various Hubbard U values (such as $U=3$, 4 , and 5 eV) on the Mn $3d$ orbitals were tested and we found that these selected U values had little effect on the structural, magnetic, and electronic properties. Thus, in this work, we adopt $U=4$ eV as in Refs. [4, 34]. From Table I, we can see that the energy of nonmagnetic (NM) state is much higher than those of other magnetic configurations, indicating that these structures all have magnetic interactions. Further, our calculations show that the FM order has the lowest energy among various magnetic configurations, suggesting that the magnetic ground state of $\text{MnX}_2\text{B}_2\text{T}_6\text{-B}$ monolayers is the FM state with an out-of-plane easy magnetization axis. Moreover, the seven $\text{MnX}_2\text{B}_2\text{T}_6\text{-B}$ monolayers in the FM ground state all exhibit good FM semiconductor properties in the presence of spin-orbit coupling (SOC) [see Fig. S4 in the SM], which may have potential applications in spintronic devices [35, 36].

The crystal structures of $\text{MnX}_2\text{B}_2\text{T}_6\text{-B}$ [Fig. 1(d)] and $\text{MnX}_2\text{B}_2\text{T}_6\text{-A}$ [Fig. 1(c)] bulks are very similar and have the same space group D_{3d}^5 (No. 166), both of which are formed by ABC stacking of 11 atomic-layers building blocks along the c -axis via the vdW interaction. However, their difference in the structure is that the X (Ge, Sn, or Pb) and B (Sb or Bi) atoms exchange positions with each other. Obviously, this is derived from the difference between their parent $X_2B_2T_5\text{-B}$ [Fig. 1(b)] and $X_2B_2T_5\text{-A}$ [Fig. 1(a)] structures. For instance, $\text{Pb}_2\text{Bi}_2\text{Te}_5\text{-A}$ and $\text{Pb}_2\text{Bi}_2\text{Te}_5\text{-B}$, which have been pre-

Table I. The crystal structure information and magnetic properties of seven $\text{MnX}_2\text{B}_2\text{T}_6\text{-B}$ monolayers, including the in-plane lattice constants optimized in the respective ferromagnetic (FM) ground state, the bond angles (Mn- T -Mn) connecting two nearest Mn atoms, the energy differences (ΔE) of various typical magnetic configurations (the nonmagnetic (NM), FM, single-row AFM (SR-AFM), and double-row AFM (DR-AFM) states) with respect to the FM state in the absence of SOC, the energy differences ($\Delta FM_{\text{B-A}}$) between the FM $\text{MnX}_2\text{B}_2\text{T}_6\text{-B}$ and the FM $\text{MnX}_2\text{B}_2\text{T}_6\text{-A}$ monolayers, the local magnetic moments (M_a), and the energy difference (magnetic anisotropy energy (MAE)) between the in-plane and out-of-plane FM states calculated with the SOC.

Monolayers	Lattice constants $a = b$ (Å)	Angles ($^\circ$) Mn- T -Mn	Without SOC ΔE (meV/Mn)					With SOC	
			NM	FM	SR-AFM	DR-AFM	$\Delta FM_{\text{B-A}}$	M_a (μ_B)	MAE (meV)
$\text{MnGe}_2\text{Sb}_2\text{Se}_6\text{-B}$	4.03	92.7	4357.2	0.0	3.1	0.8	-186.1	4.56	0.04
$\text{MnGe}_2\text{Sb}_2\text{Te}_6\text{-B}$	4.28	92.0	4312.8	0.0	4.7	2.0	-73.4	4.54	0.03
$\text{MnGe}_2\text{Bi}_2\text{Se}_6\text{-B}$	4.08	93.7	4410.2	0.0	3.2	1.0	-212.0	4.57	0.02
$\text{MnGe}_2\text{Bi}_2\text{Te}_6\text{-B}$	4.33	92.8	4365.1	0.0	3.6	1.7	-98.3	4.55	0.04
$\text{MnSn}_2\text{Sb}_2\text{Te}_6\text{-B}$	4.38	93.8	4301.6	0.0	4.8	2.2	-154.6	4.56	0.11
$\text{MnSn}_2\text{Bi}_2\text{Te}_6\text{-B}$	4.43	94.7	4358.8	0.0	4.2	1.8	-185.2	4.56	0.01
$\text{MnPb}_2\text{Bi}_2\text{Te}_6\text{-B}$	4.46	95.2	4414.9	0.0	2.4	0.4	-505.2	4.57	0.08

pared experimentally [20, 21], exchange the positions of Pb and Bi atoms. It is worth noting that the $\text{Pb}_2\text{Bi}_2\text{Te}_5\text{-B}$ is a stable structural form of $\text{Pb}_2\text{Bi}_2\text{Te}_5\text{-A}$ in the range of temperatures 1000 K [22]. Therefore, we focus on the stable parent $X_2\text{B}_2\text{T}_5\text{-B}$ structures. A natural question is whether the $\text{MnX}_2\text{B}_2\text{T}_6\text{-B}$ family derived from this stable parent $X_2\text{B}_2\text{T}_5\text{-B}$ can have a stable structural form with lower energy than that of the $\text{MnX}_2\text{B}_2\text{T}_6\text{-A}$ family? To this end, we firstly searched the MnBi_2Te_4 system based on the USPEX evolutionary algorithm and quickly obtained the real synthesized MnBi_2Te_4 crystals [37] with the space group $R\bar{3}m$ [see Fig. S3 in the SM], which confirmed the effectiveness of the method. After that, we carried out a systematic search for the $\text{MnPb}_2\text{Bi}_2\text{Te}_6$ system, and found that the energy of $\text{MnPb}_2\text{Bi}_2\text{Te}_6\text{-B}$ phase is indeed lower than that of the $\text{MnPb}_2\text{Bi}_2\text{Te}_6\text{-A}$ phase [18] by nearly 526.9 meV/Mn (see Table II). The $\text{MnPb}_2\text{Bi}_2\text{Te}_6\text{-B}$ phase is located at the lowest energy (Fig. 2), showing that the $\text{MnPb}_2\text{Bi}_2\text{Te}_6\text{-B}$ phase is the ground state of the $\text{MnPb}_2\text{Bi}_2\text{Te}_6$ system.

After confirming the intralayer FM ground state of $\text{MnX}_2\text{B}_2\text{T}_6\text{-B}$ monolayer, we only need to consider the interlayer magnetic interaction to determine the magnetic ground state of $\text{MnX}_2\text{B}_2\text{T}_6\text{-B}$ bulks. From Table II, we can see that $\text{MnGe}_2\text{Sb}_2\text{Se}_6\text{-B}$ and $\text{MnGe}_2\text{Bi}_2\text{Se}_6\text{-B}$ bulk exhibit the A-type AFM magnetic ground state similar to MnBi_2Te_4 [3–5], while the remaining five $\text{MnX}_2\text{B}_2\text{T}_6\text{-B}$ bulks all have the FM ground state. From the magnetic anisotropy energy (MAE), the seven bulk compounds all host the same out-of-plane easy axis of magnetization as their monolayers. Meanwhile, we note that the energies of the seven $\text{MnX}_2\text{B}_2\text{T}_6\text{-B}$ bulks are 42.9–526.9 meV/Mn lower than those of the $\text{MnX}_2\text{B}_2\text{T}_6\text{-A}$ bulks in their respective ground states, suggesting that $\text{MnX}_2\text{B}_2\text{T}_6\text{-B}$ is the stable structural form of the $\text{MnX}_2\text{B}_2\text{T}_6$ system.

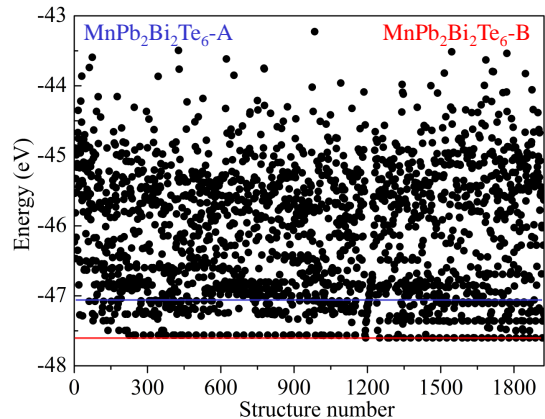


Figure 2. (Color online) Total energy evolution for the $\text{MnPb}_2\text{Bi}_2\text{Te}_6$ system during the magnetic evolutionary search. The red and blue lines represent the most stable structure $\text{MnPb}_2\text{Bi}_2\text{Te}_6\text{-B}$ and metastable $\text{MnPb}_2\text{Bi}_2\text{Te}_6\text{-A}$, respectively.

The most interesting property of the $\text{MnX}_2\text{B}_2\text{T}_6\text{-B}$ bulks is its electronic band structure with the abundant topological phases. Figure 3 shows the spin-polarized band structures and density of states (DOS) of $\text{MnSn}_2\text{Sb}_2\text{Te}_6\text{-B}$ and $\text{MnPb}_2\text{Bi}_2\text{Te}_6\text{-B}$ bulks in the FM ground state. We can find that they both are FM semiconductors with narrow band gaps (0.23 and 0.61 eV), and their energy bands near the top of valence bands mainly come from the contributions of the p orbitals of Te, Sb/Bi, and Sn/Pb atoms. The spin-polarized band structures of the other five $\text{MnX}_2\text{B}_2\text{T}_6\text{-B}$ bulks in their respective ground states are shown in Fig. S5 of the SM.

When the SOC effect is taken into account, the band structure of $\text{MnSn}_2\text{Sb}_2\text{Te}_6\text{-B}$ bulk in the FM ground state with an out-of-plane easy magnetization axis is shown

Table II. The structure information, magnetic, and topological properties of seven bulk compounds of the $\text{MnX}_2\text{B}_2\text{T}_6\text{-B}$ family, including the lattice constants optimized in their respective ground states, the bond angles (Mn- T -Mn) connecting two nearest Mn atoms, the local magnetic moments (M_a), the energy differences ($\Delta E_{\text{B-A}}$) of the $\text{MnX}_2\text{B}_2\text{T}_6\text{-B}$ phase with respect to the $\text{MnX}_2\text{B}_2\text{T}_6\text{-A}$ phase, the energy differences ($\Delta E_{\text{AFM-FM}}$) between the A-type AFM and FM orders, the energy differences (magnetic anisotropy energy (MAE)) between the in-plane and out-of-plane spin orientations in their respective ground states, the number of occupied bands with even and odd parity eigenvalues (n_{occ}^+, n_{occ}^-) at the eight inversion-invariant momentum points (Λ_α) in the presence of SOC, and the parity-based Z_4 invariant.

Bulks	Lattice constants		Angles ($^\circ$) Mn- T -Mn (μ_B)	M_a	$\Delta E_{\text{B-A}}$ meV/Mn	$\Delta E_{\text{AFM-FM}}$ meV/Mn	MAE (meV)	Λ_α				Z_4
	$a=b$ (\AA)	c (\AA)						Γ (0,0,0)	L (0, π ,0)	F (π , π ,0)	Z (π , π , π)	
$\text{MnGe}_2\text{Sb}_2\text{Se}_6\text{-B}$	4.00	57.69	93.0	4.55	-149.0	-0.097	0.41	(86,88)	(87,87)	(86,88)	(87,87)	0
$\text{MnGe}_2\text{Sb}_2\text{Te}_6\text{-B}$	4.27	60.91	92.4	4.53	-56.6	0.043	0.17	(43,44)	(43,44)	(43,44)	(43,44)	0
$\text{MnGe}_2\text{Bi}_2\text{Se}_6\text{-B}$	4.06	58.17	94.0	4.56	-131.6	-0.095	0.02	(106,108)	(107,107)	(106,108)	(107,107)	0
$\text{MnGe}_2\text{Bi}_2\text{Te}_6\text{-B}$	4.34	61.68	93.9	4.54	-42.9	0.038	0.12	(55,52)	(53,54)	(53,54)	(53,54)	2
$\text{MnSn}_2\text{Sb}_2\text{Te}_6\text{-B}$	4.36	62.05	94.4	4.54	-193.4	0.14	0.10	(44,43)	(43,44)	(43,44)	(43,44)	1
$\text{MnSn}_2\text{Bi}_2\text{Te}_6\text{-B}$	4.42	62.46	95.2	4.55	-196.2	0.125	0.43	(55,52)	(53,54)	(53,54)	(53,54)	2
$\text{MnPb}_2\text{Bi}_2\text{Te}_6\text{-B}$	4.44	63.20	95.9	4.56	-526.9	0.035	0.29	(55,52)	(53,54)	(53,54)	(53,54)	2

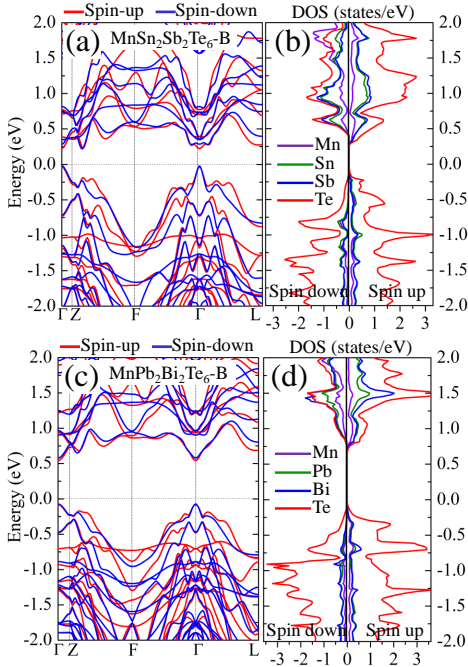


Figure 3. (Color online) Spin-polarized band structures and density of states (DOS) of the bulk compounds $\text{MnSn}_2\text{Sb}_2\text{Te}_6\text{-B}$ and $\text{MnPb}_2\text{Bi}_2\text{Te}_6\text{-B}$ calculated without the SOC in the ferromagnetic ground state.

in Fig. 4(a). One can see that it has only a minimal number of two type-I Weyl points along the $Z\text{-}\Gamma\text{-}Z$ high-symmetry path near the Fermi level without other interfering bands [inset of Fig. 4(a)]. The band crossings are mainly caused by the hybridization between the p orbitals of the Te and Sb atoms and protected by the C_3 rotational symmetry. Our Wannier charge center (WCC) calculations show that the two Weyl points (WP_1 and

WP_2) exhibit opposite chirality carrying the topological charges of +1 and -1 [Fig. 4(b)], respectively, indicating that $\text{MnSn}_2\text{Sb}_2\text{Te}_6\text{-B}$ is an ideal topological WSM. In addition, the calculated Chern numbers $C = 1$ at $k_z = 0$ plane and $C = 0$ at $k_z = \pi$ plane are also consistent with the feature of an ideal WSM. On the other hand, we also investigated the effect of strain on the topological properties of $\text{MnSn}_2\text{Sb}_2\text{Te}_6\text{-B}$ bulk by applying uniaxial stress from -5% (compression) to 5% (tensile) along the c -axis. As shown in Fig. 4(c), for $\text{MnSn}_2\text{Sb}_2\text{Te}_6\text{-B}$ bulk in the FM ground state, the energy gap between the valence band maximum (VBM) and the conduction band minimum (CBM) at the Γ point increases monotonically with the increase of compressive stress and becomes an FM axion insulator (AXI). However, under tensile stress within 3% it is still a WSM with a single pair of Weyl points. Once the tensile stress exceeds 3%, the system becomes a trivial FM insulator (FMI). Figure 4(d) shows the projected band structure with orbital weights for $\text{MnPb}_2\text{Bi}_2\text{Te}_6\text{-B}$ bulk in the FM ground state with an out-of-plane easy magnetization axis, we can see that there is a band inversion between the p orbitals of Te and Bi atoms at the Γ point near the Fermi level, indicating that the $\text{MnPb}_2\text{Bi}_2\text{Te}_6\text{-B}$ bulk may have nontrivial topological properties. For the other five $\text{MnX}_2\text{B}_2\text{T}_6\text{-B}$ bulks in their respective ground states, their band structures calculated with the SOC are shown in Fig. S6 of the SM.

Since the $\text{MnX}_2\text{B}_2\text{T}_6\text{-B}$ family has the inversion symmetry under different ground state magnetic configurations, a parity-based Z_4 symmetry indicator can be used to characterize the topological properties of $\text{MnX}_2\text{B}_2\text{T}_6\text{-B}$ family. The Z_4 invariant is given by [38–40]

$$Z_4 = \sum_{\alpha=1}^8 \sum_{n=1}^{n_{occ}} \frac{1 + \xi_n(\Lambda_\alpha)}{2} \text{ mod } 4, \quad (1)$$

where Λ_α are the eight inversion-symmetric crystal mo-

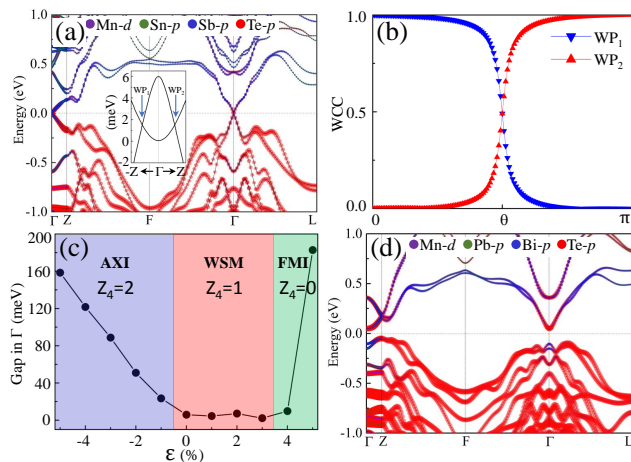


Figure 4. (Color online) Band structures with orbital weights for (a) $\text{MnSn}_2\text{Sb}_2\text{Te}_6\text{-B}$ and (d) $\text{MnPb}_2\text{Bi}_2\text{Te}_6\text{-B}$ bulk materials calculated with the SOC in the out-of-plane FM ground states. Single pair of Weyl points along the $-\text{Z}-\Gamma\text{-Z}$ path near the Fermi level are shown in inset (a). Two ideal Weyl points (WP_1 and WP_2) are separated 0.06 \AA^{-1} along the k_z direction, which is comparable to MnBi_2Te_4 in the FM state. (b) Motions of the sum of Wannier charge centers (WCCs) on a sphere enclosing each Weyl point in the BZ. (c) The energy gap between the lowest unoccupied state and the highest occupied state at Γ as a function of stress along the c -axis.

menta, $\xi_n(\Lambda_\alpha)$ is the parity eigenvalue (+1 or -1) of the n th occupied band at the Λ_α , and n_{occ} is the total number of occupied bands. $Z_4=1$ or 3 corresponds to a Weyl semimetal (WSM) phase [38], while $Z_4=2$ indicates an axion insulator (AXI) [the axion angle $\theta = \pi$] in the case of the Chern numbers on all the 2D planes in the BZ are zeros [41, 42]. From Table II, we can find that the Z_4 invariant of $\text{MnSn}_2\text{Sb}_2\text{Te}_6\text{-B}$ equals to 1, indicating that it is a WSM, which is consistent with our calculated band structures [Fig. 4(a)] and WCCs [Fig. 4(b)]. While the $\text{MnGe}_2\text{Bi}_2\text{Te}_6\text{-B}$, $\text{MnSn}_2\text{Bi}_2\text{Te}_6\text{-B}$, and $\text{MnPb}_2\text{Bi}_2\text{Te}_6\text{-B}$ bulks correspond to $Z_4=2$, the calculated Chern numbers at $k_z = 0$ and $k_z = \pi$ planes both equal to 0, implying that they are a class of FM axion insulators. Furthermore, the Z_4 invariants of $\text{MnGe}_2\text{Sb}_2\text{Se}_6\text{-B}$, $\text{MnGe}_2\text{Sb}_2\text{Te}_6\text{-B}$ and $\text{MnGe}_2\text{Bi}_2\text{Se}_6\text{-B}$ equal to 0, suggesting that they are a class of trivial insulators.

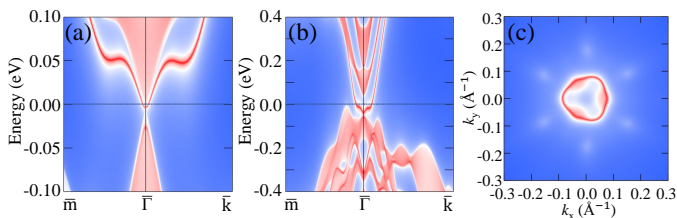


Figure 5. (Color online) Surface energy bands of the semi-infinite (111) surface of (a) $\text{MnSn}_2\text{Sb}_2\text{Te}_6\text{-B}$ and (b) $\text{MnPb}_2\text{Bi}_2\text{Te}_6\text{-B}$. (c) A triangular Fermi surface on the (111) surface of $\text{MnPb}_2\text{Bi}_2\text{Te}_6\text{-B}$.

Both WSMs and FM axion insulators exhibit unique topological surface states. Considering that $\text{MnX}_2\text{B}_2\text{T}_6\text{-B}$ bulks are formed by ABC stacking of 11 atomic layers building blocks along the c -axis via the vdW interaction, the (111) surface of their primitive cells located in the vdW gap is their natural cleavage plane. So, we calculated the surface states for the (111) surfaces of $\text{MnSn}_2\text{Sb}_2\text{Te}_6\text{-B}$ and $\text{MnPb}_2\text{Bi}_2\text{Te}_6\text{-B}$. We can find that the two Weyl points (WP_1 and WP_2) of $\text{MnSn}_2\text{Sb}_2\text{Te}_6\text{-B}$ bulk are exactly projected to the same point $\bar{\Gamma}$ on the (111) surface, thus the two surface Fermi arcs are displayed at the $\bar{\Gamma}$ point [Fig. 5(a)]. However, for axion insulator, in addition to the above axion angle $\theta = \pi$, a gapped surface state is also required. We take $\text{MnPb}_2\text{Bi}_2\text{Te}_6\text{-B}$ as an example to calculate the surface bands in the projected (111) surface [see Fig. 5(b)]. One can see that the surface states at the $\bar{\Gamma}$ point near the Fermi level do open an energy gap ($\sim 20 \text{ meV}$) and are accompanied by a triangular Fermi surface [see Fig. 5(c)], which is similar to the surface state of $\text{MnGe}_2\text{Sb}_2\text{Te}_6\text{-A}$ that we previously reported [18]. Notably, $\text{MnPb}_2\text{Bi}_2\text{Te}_6\text{-B}$ has only the gapped surface state at the Fermi level without other interfering bulk states.

Discussion: It is well known that the search for the ideal Weyl semimetals with a single pair of Weyl points and the intrinsic FM axion insulators in magnetic materials with highly desirable topological states has been a challenging task. Despite a long search, their candidates are still rare so far [17–19]. Fortunately, both of the two unique topological states can be found in the $\text{MnX}_2\text{B}_2\text{T}_6\text{-B}$ family. Compared with our previous work on $\text{MnX}_2\text{B}_2\text{T}_6\text{-A}$, the $\text{MnX}_2\text{B}_2\text{T}_6\text{-B}$ family has the following advantages. First, not only the energy of the $\text{MnX}_2\text{B}_2\text{T}_6\text{-B}$ family is lower than that of the $\text{MnX}_2\text{B}_2\text{T}_6\text{-A}$ family, but also the former is the stable structural form of $\text{MnX}_2\text{B}_2\text{T}_6$ system. Second, a new topological phase emerges from the $\text{MnX}_2\text{B}_2\text{T}_6\text{-B}$ family, that is, the ideal magnetic Weyl state with only a single pair of Weyl points. Third, $\text{MnPb}_2\text{Bi}_2\text{Te}_6\text{-B}$ has only the gapped surface state at the Fermi level without other interfering bulk states. Thus, it can provide a more ideal platform for future experiments to explore the long-sought quantized magnetoelectric effect based on the FM axion insulators. Finally, we emphasize that our design scheme can provide new ideas for realizing more vdW-type magnetic topological materials.

Summary: To summarize, we propose a new class of $\text{MnX}_2\text{B}_2\text{T}_6\text{-B}$ ($X=\text{Ge, Sn, or Pb}$; $B=\text{Sb or Bi}$; $T=\text{Se or Te}$) family that is the stable structural form of the $\text{MnX}_2\text{B}_2\text{T}_6\text{-A}$ materials we reported before. We systematically investigate the stability, magnetic, electronic and topological properties of the $\text{MnX}_2\text{B}_2\text{T}_6\text{-B}$ family and find that $\text{MnX}_2\text{B}_2\text{T}_6\text{-B}$ monolayers are narrow-bandgap ferromagnetic (FM) semiconductors in their FM ground state with an out-of-plane easy magnetization axis, while $\text{MnX}_2\text{B}_2\text{T}_6\text{-B}$ bulks not only have the intrinsic FM axion insulators $\text{MnGe}_2\text{Bi}_2\text{Te}_6\text{-B}$, $\text{MnSn}_2\text{Bi}_2\text{Te}_6\text{-B}$, and $\text{MnPb}_2\text{Bi}_2\text{Te}_6\text{-B}$, but also the intrinsic WSM

MnSn₂Sb₂Te₆-B with only a single pair of Weyl points that has not appeared in the MnX₂B₂T₆-A family. Thus, the new MnX₂B₂T₆-B family can provide an ideal platform for future experiments to explore the long-sought quantized magnetoelectric effect and the intrinsic properties related to Weyl points.

ACKNOWLEDGMENTS

We wish to thank QuanSheng Wu and Wei Liu for helpful discussions. This work was supported by the National Key R&D Program of China (Grant No. 2019YFA0308603), the National Natural Science Foundation of China (Grants no. 11934020 and No. 12174443), and the Beijing Natural Science Foundation (Grant No. Z200005). Y. G is also grateful for the support of HWTECH for providing computational facilities.

-
- [1] M. M. Otrokov, I. I. Klimovskikh, H. Bentmann, D. Estyunin, A. Zeugner, Z. S. Aliev, S. Gaß, A. Wolter, A. Koroleva, and A. M. Shikin, *Nature* **576**, 416 (2019).
- [2] Y. Deng, Y. Yu, M. Z. Shi, Z. Guo, Z. Xu, J. Wang, X. H. Chen, and Y. Zhang, *Science* **367**, 895 (2020).
- [3] Y. Gong, J. Guo, J. Li, K. Zhu, M. Liao, X. Liu, Q. Zhang, L. Gu, L. Tang, and X. Feng, *Chin. Phys. Lett.* **36**, 076801 (2019).
- [4] J. Li, Y. Li, S. Du, Z. Wang, B.-L. Gu, S.-C. Zhang, K. He, W. Duan, and Y. Xu, *Sci. Adv.* **5**, eaaw5685 (2019).
- [5] D. Zhang, M. Shi, T. Zhu, D. Xing, H. Zhang, and J. Wang, *Phys. Rev. Lett.* **122**, 206401 (2019).
- [6] M. M. Otrokov, I. P. Rusinov, M. Blanco-Rey, M. Hoffmann, A. Y. Vyazovskaya, S. V. Eremeev, A. Ernst, P. M. Echenique, A. Arnau, and E. V. Chulkov, *Phys. Rev. Lett.* **122**, 107202 (2019).
- [7] C. Liu, Y. Wang, H. Li, Y. Wu, Y. Li, J. Li, K. He, Y. Xu, J. Zhang, and Y. Wang, *Nat. Mater.* **19**, 522 (2020).
- [8] Y.-J. Hao, P. Liu, Y. Feng, X.-M. Ma, E. F. Schwier, M. Arita, S. Kumar, C. Hu, M. Zeng, and Y. Wang, *Phys. Rev. X* **9**, 041038 (2019).
- [9] A. Zeugner, F. Nietschke, A. U. Wolter, S. Gaß, R. C. Vidal, T. R. Peixoto, D. Pohl, C. Damm, A. Lubk, and R. Hentrich, *Chem. Mater.* **31**, 2795 (2019).
- [10] H. Li, S.-Y. Gao, S.-F. Duan, Y.-F. Xu, K.-J. Zhu, S.-J. Tian, J.-C. Gao, W.-H. Fan, Z.-C. Rao, and J.-R. Huang, *Phys. Rev. X* **9**, 041039 (2019).
- [11] Y. Chen, L. Xu, J. Li, Y. Li, H. Wang, C. Zhang, H. Li, Y. Wu, A. Liang, and C. Chen, *Phys. Rev. X* **9**, 041040 (2019).
- [12] B. Li, J.-Q. Yan, D. M. Pajerowski, E. Gordon, A.-M. Nedić, Y. Sizyuk, L. Ke, P. P. Orth, D. Vaknin, and R. J. McQueeney, *Phys. Rev. Lett.* **124**, 167204 (2020).
- [13] S. Zhang, R. Wang, X. Wang, B. Wei, B. Chen, H. Wang, G. Shi, F. Wang, B. Jia, and Y. Ouyang, *Nano Lett.* **20**, 709 (2019).
- [14] J. Li, C. Wang, Z. Zhang, B.-L. Gu, W. Duan, and Y. Xu, *Phys. Rev. B* **100**, 121103(R) (2019).
- [15] Y. Wan, J. Li, and Q. Liu, *Natl. Sci. Rev.* (2022).
- [16] B. A. Bernevig, *Nat. Phys.* **11**, 698 (2015).
- [17] C. Hu, L. Ding, K. N. Gordon, B. Ghosh, H.-J. Tien, H. Li, A. G. Linn, S.-W. Lien, C.-Y. Huang, and S. Mackey, *Sci. Adv.* **6**, eaba4275 (2020).
- [18] Y. Gao, K. Liu, and Z.-Y. Lu, *Phys. Rev. Research* **4**, 023030 (2022).
- [19] S. Nie, T. Hashimoto, and F. B. Prinz, *Phys. Rev. Lett.* **128**, 176401 (2022).
- [20] I. Petrov and R. Imamov, *Sov. Phys. Crystallogr.* **14**, 593 (1970).
- [21] A. Chatterjee and K. Biswas, *Angew. Chem., Int. Ed.* **127**, 5715 (2015).
- [22] W. Ma, M.-C. Record, J. Tian, and P. Boulet, *Phys. Chem. Chem. Phys.* **23**, 11300 (2021).
- [23] I. Silkin, Y. M. Koroteev, S. V. Eremeev, G. Bihlmayer, and E. V. Chulkov, *JETP Lett.* **94**, 217 (2011).
- [24] P. E. Blöchl, *Phys. Rev. B* **50**, 17953 (1994).
- [25] G. Kresse and J. Furthmüller, *Comput. Mater. Sci.* **6**, 15 (1996).
- [26] J. P. Perdew, K. Burke, and M. Ernzerhof, *Phys. Rev. Lett.* **77**, 3865 (1996).
- [27] S. Grimme, J. Antony, S. Ehrlich, and H. Krieg, *J. Chem. Phys.* **132**, 154104 (2010).
- [28] H. J. Monkhorst and J. D. Pack, *Phys. Rev. B* **13**, 5188 (1976).
- [29] Hongzhiwei Technology, Device Studio, Version 2021A, China, 2021. Available online: <https://iresearch.net.cn/cloudSoftware>.
- [30] A. A. Mostofi, J. R. Yates, Y.-S. Lee, I. Souza, D. Vanderbilt, and N. Marzari, *Comput. Phys. Commun.* **178**, 685 (2008).
- [31] Q. Wu, S. Zhang, H.-F. Song, M. Troyer, and A. A. Soluyanov, *Comput. Phys. Commun.* **224**, 405 (2018).
- [32] A. R. Oganov and C. W. Glass, *J. Chem. Phys.* **124**, 244704 (2006).
- [33] A. O. Lyakhov, A. R. Oganov, H. T. Stokes, and Q. Zhu, *Comput. Phys. Commun.* **184**, 1172 (2013).
- [34] P. Li, J. Yu, Y. Wang, and W. Luo, *Phys. Rev. B* **103**, 155118 (2021).
- [35] A. H. MacDonald, P. Schiffer, and N. Samarth, *Nat. Mater.* **4**, 195 (2005).
- [36] S. Das Sarma, *Nat. Mater.* **2**, 292 (2003).
- [37] D. S. Lee, T.-H. Kim, C.-H. Park, C.-Y. Chung, Y. S. Lim, W.-S. Seo, and H.-H. Park, *CrystEngComm* **15**, 5532 (2013).
- [38] A. M. Turner, Y. Zhang, R. S. K. Mong, and A. Vishwanath, *Phys. Rev. B* **85**, 165120 (2012).
- [39] S. Ono and H. Watanabe, *Phys. Rev. B* **98**, 115150 (2018).
- [40] H. Watanabe, H. C. Po, and A. Vishwanath, *Sci. Adv.* **4**, eaat8685 (2018).
- [41] S. Huan, S. Zhang, Z. Jiang, H. Su, H. Wang, X. Zhang, Y. Yang, Z. Liu, X. Wang, and N. Yu, *Phys. Rev. Lett.* **126**, 246601 (2021).
- [42] Y. Xu, Z. Song, Z. Wang, H. Weng, and X. Dai, *Phys. Rev. Lett.* **122**, 256402 (2019).